THE JOURNAL OF BIOLOGICAL CHEMISTRY VOL. 286, NO. 2, pp. 1381–1388, January 14, 2011

Characterization of the Oligomeric Structure of the Ca^{2+}-activated Cl^- Channel Ano1/TMEM16A*

Received for publication, August 12, 2010, and in revised form, October 18, 2010 Published, JBC Papers in Press, November 5, 2010, DOI 10.1074/jbc.M110.174847

John T. Sheridan[‡1,2], **Erin N. Worthington**[§1], **Kuai Yu**[¶], **Sherif E. Gabriel**[§], **H. Criss Hartzell**[¶], **and Robert Tarran**[‡§3]

From the [‡]*Department of Cell and Molecular Physiology and the* [§]*Cystic Fibrosis/Pulmonary Research and Treatment Center, University of North Carolina, North Carolina, Chapel Hill 27599 and the* [¶]*Department of Cell Biology, Emory University School of Medicine, Atlanta, Georgia 30322*

Members of the Anoctamin (Ano)/TMEM16A family have recently been identified as essential subunits of the Ca^{2+}-activated chloride channel (CaCC). For example, Ano1 is highly expressed in multiple tissues including airway epithelia, where it acts as an apical conduit for transepithelial Cl^- secretion and helps regulate lung liquid homeostasis and mucus clearance. However, little is known about the oligomerization of this protein in the plasma membrane. Thus, utilizing mCherry- and eGFP-tagged Ano1 constructs, we conducted biochemical and Förster resonance energy transfer (FRET)-based experiments to determine the quaternary structure of Ano1. FRET and co-immunoprecipitation studies revealed that tagged Ano1 subunits directly associated before they reached the plasma membrane. This association was not altered by changes in cytosolic Ca^{2+}, suggesting that this is a fixed interaction. To determine the oligomeric structure of Ano1, we performed chemical cross-linking, non-denaturing PAGE, and electromobility shift assays, which revealed that Ano1 exists as a dimer. These data are the first to probe the quaternary structure of Ano1. Understanding the oligomeric nature of Ano1 is an essential step in the development of therapeutic drugs that could be useful in the treatment of cystic fibrosis.

Ca^{2+}-activated Cl^- channels (CaCCs)[4] play essential roles in many physiological processes including epithelial secretion (1), olfactory transduction (2–4), photoreceptor adaptation (5), regulation of smooth muscle contraction (6), neuronal and cardiac action potential waveform and firing frequency (7), and nociception (8). Because of their physiological significance, CaCCs have attracted attention for decades (9, 10). However, their molecular composition has remained elusive until recently when three laboratories independently identified members of the Anoctamin 1 (Ano1) family, also known as the transmembrane protein 16 (TMEM16) family, as essential subunits of CaCCs (11–13). Ano1/TMEM16A is highly expressed in secretory epithelial tissues including ductal glands, superficial epithelia of the airway, and oviduct, where it has been implicated to play a key role in calcium-dependent chloride secretion (11, 13–16). Ano1 has attracted particular attention in the airways, because it has been suggested that activating this channel might be therapeutically beneficial for treating cystic fibrosis (CF) patients (15). The cystic fibrosis conductance regulator (CFTR) chloride channel is absent or defective in CF epithelia, leaving Ano1 as a potential alternative pathway to effect transepithelial Cl^- secretion.

The anoctamin family consists of 10 members, all of which are predicted to have 8 transmembrane domains with cytosolic N and C termini. Ano1 is regulated by both intracellular Ca^{2+} and by voltage, in a similar fashion to native CaCCs (17), but the mechanisms are not well defined (18). The homology between family members suggests that other Anos may also function as CaCCs (19) and Ano2 has also been shown to mediate the Ca^{2+}-activated Cl^- current in olfactory epithelium and photoreceptor synapses (4, 5, 20). With the possible exception of Ano8 and Ano10, anoctamins are also predicted to have a re-entrant loop between transmembrane domains 5 and 6 that may contribute toward Cl^- selectivity (21, 22).

A common property of ion channels is their oligomeric nature, which may be homo- or hetero-oligomeric (23). For example, activation of the MthKCa^{2+}-activated K^+ channel from *Methanobacterium thermoautrophicum* involves oligomerization of 4 subunits (24) and it has been suggested that the mammalian Maxi-K K^+ channel is activated by a similar mechanism (25). Activation of CFTR Cl^- channels involves dimerization of nucleotide binding domains (26), although whether CFTR enters the plasma membrane as a monomer or a dimer remains controversial (27, 28). A first step in understanding how Ano1 is gated and regulated requires knowing whether the channel exists as a monomer or an oligomer and, if it oligomerizes, the number of interacting subunits. Because little is known about how Ano1 forms a Cl^- conducting channel in the apical membrane, we have used biochemical techniques and Förster resonance energy transfer (FRET)-based approaches to investigate its subunit assembly.

* This work was supported, in whole or in part, by National Institutes of Health Grants HL084934, HL034322, EY0148852, and GM60448, the Cystic Fibrosis Foundation, and the Children's Healthcare of Atlanta Center for Cystic Fibrosis Research.

[1] Both authors contributed equally to this work.

[2] Supported in part by the Howard Hughes Medical Institute Med-Into-Grad University of North Carolina Program in Translational Medicine.

[3] To whom correspondence should be addressed. Tel.: 919-966-7052; Fax: 919-966-5178; E-mail: tarran@med.unc.edu.

[4] The abbreviations used are: CaCC, Ca^{2+}-activated Cl^- channel; Ano1, anoctamin 1; TMEM16, transmembrane protein 16; CF, cystic fibrosis; mCherry, monomeric cherry; A2BR, adenosine 2b receptor; CFTR, cystic fibrosis transmembrance conductance regulator; ENaC, epithelial sodium channel; eGFP, enhanced GFP; BisTris, 2-[bis(2-hydroxyethyl)amino]-2-(hydroxymethyl)propane-1,3-diol.

TABLE 1
Primers used in RT-PCR to detect endogenous anoctamin expression in HEK293 cells

Gene	Sense	Antisense
Ano1	GCGTCCACATCATCAACATC	ATCCTCGTGGTAGTCCATCG
Ano2	TGCCTACCACTACCGGAAAC	ACTTCTTTGCAATGCTGCCT
Ano3	AAACCTGAACCACATCAGCC	TCTTCCCAAAAAGAAAGCGA
Ano4	CATGGGAAGTCCTTGGAAGA	GCCATTGGTAAGCAAACGAT
Ano5	ACACTTCACCAGAATTGGGC	GAAGCTGCTGCTGTTCCTCT
Ano6	CAGTTTGGGTTCGTCACCTT	AGTACGGGTTTCCCTTGCTT
Ano7	CTACTCCTGCCGGTTCAGAG	GTTCCTGCGTGGGTATGTCT
Ano8	ACTTCGCTCTGCTCCTCAAG	CTTCATGACGTTGTTGGGTG
Ano9	TGGAGATCAGCACCTGTGAG	CGAAGTTCACGATTCGGATT
Ano10	GAGGTGCCCAGTTGTTGTTT	CCGAGTGTACCAGGTGTCCT

EXPERIMENTAL PROCEDURES

Cell Culture—Human excess donor lungs and excised recipient lungs were obtained at the time of lung transplantation from portions of the main stem or lumbar bronchi and cells were harvested by enzymatic digestion as previously described under a protocol approved by the University of North Carolina School of Medicine IRB. Human bronchial epithelia cells were transfected with Ano1 constructs in suspension using the Amaxa system (Lonza) as per the manufacturer's instructions and were cultured overnight on 30-mm glass coverslips before imaging. HEK293 cells were maintained in minimum essential medium supplemented with 10% fetal bovine serum and 1× penicillin/streptomycin solution. HEK293 cells were typically used 2–3 days after seeding on 30-mm glass coverslips. Cultures that were ~75% confluent were transfected for 4–6 h using Lipofectamine 2000 (Invitrogen) as per the manufacturer's instructions and allowed to incubate in 5% CO_2 at 37 °C overnight before use.

Ano1 Constructs and RT-PCR—Mouse Ano1 C-terminal fused with enhanced GFP (Ano1-eGFP) was kindly provided by Dr. Uhtaek Oh (Seoul National University, Korea; variant containing *a* and *c* alternative splice sequences, UniProtKB accession number Q8BHY3.2). Ano1-eGFP is in the pEGFP vector (Clontech). The Ano1-mCherry construct was made by replacing eGFP with monomeric Cherry (mCherry, Clontech). In both constructs, the fluorescent tag was separated from the C terminus of Ano1 by a 17-amino acid linker (RILQSTVPRARDPPVAT) to ensure that the fluorescent protein did not affect Ano1 function as previously described (29). The HA-tagged $P2Y_2$ receptor construct was donated by Kendall Harden (Department of Pharmacology, UNC, Chapel Hill, NC) (30). Endogenous expression of all Ano family members (Ano1–10) was determined by RT-PCR using primers as listed in Table 1.

Patch Clamping—Whole cell patch clamp recording was performed with an Axopatch 200B amplifier as previously reported (31). The voltage clamp protocol consisted of 750 ms duration steps from a 0-mV holding potential to various potentials between −100 and +100 mV in 20-mV increments. Fluorescent cells were chosen for recording. The pipette solution contained (in mM): 146 CsCl, 2 $MgCl_2$, 5 EGTA, 0 or 5.0143 $CaCl_2$ to make free [Ca^{2+}] of 0 or 1 μM, 10 sucrose, and 8 HEPES, pH 7.3, adjusted with *N*-methyl-D-glucamine. The standard external solution contained (in mM): 140 NaCl, 4 KCl, 2 $CaCl_2$, 1 $MgCl_2$, 10 glucose, 10 HEPES, pH 7.3.

Acceptor Photobleaching FRET—FRET was performed using a Leica SP5 confocal microscope with a ×63 glycerol immersion objective. The donor (eGFP) was excited at 488 nm and emission collected from 495 to 549 nm, and the acceptor (mCherry) was excited at 561 nm and emission collected from 580 to 654 nm. FRET was measured by the acceptor photobleaching method and analyzed using ImageJ (NIH Freeware). The FRET efficiency (%*E*) was calculated as: $((donor^{postbleach} - donor^{prebleach})/donor^{postbleach}) \times 100$.

Measurements of $Ca^{2+}{}_i$—All cultures were loaded with Fura-2-AM (5 μM at 37 °C for 40 min) and imaged with a 60 × 1.2 NA H_2O objective on a Nikon Ti-S microscope. $Ca^{2+}{}_i$ measurements were obtained using an Orca camera (Hamamatsu) and Fura-2 fluorescence was acquired alternately at 340 and 380 nm (emission >450 nm) using Ludl filter wheels with Compix sPCI software. At each excitation wavelength (340 or 380 nm), background light levels were measured by exposing cells to digitonin (15 μM) and $MnCl_2$ (10 mM) and subtracting the emission from the corresponding signal measured in Fura-2-loaded cells before taking the ratio (340/380) (32).

Imaging of the Actin Cytoskeleton—For labeling of actin, HEK293 cells were grown on glass coverslips. Cells were incubated with 1 μM cytochalasin D or vehicle (0.1% DMSO) for 30 min and then fixed in 4% paraformaldehyde for 10 min at room temperature. After washing 3 times in PBS, cells were permeabilized by a 10-min exposure to 1% Triton X-100. After washing 3 times, cells were incubated with Alexa 488-phalloidin (Invitrogen) for 30 min, followed by a deep red HCS cell mask (Invitrogen) for 30 min as per the manufacturer's instructions. Fixed cells were then imaged immediately using the Leica SP5 confocal microscope.

Co-immunoprecipitation and Western Blotting—Co-immunoprecipitation was performed in HEK293 cells transfected with Ano1-mCherry and Ano1-eGFP, adenosine-2B receptor-eGFP (A2BR-eGFP), or eGFP. Cells were lysed in 600 μl of Nonidet P-40 lysis buffer (0.09% Nonidet P-40, 50 mM Tris-HCl, pH 7.4, 10 mM $NaMoO_4$, 150 mM NaCl) supplemented with 1× complete EDTA-free protease inhibitors (Roche). Lysates were then centrifuged at 16,000 × *g* for 10 min at 4 °C and the supernatants were collected. Protein concentrations were determined by the BCA protein assay kit (Pierce) and equal amounts of protein (800 μg) were diluted to 1.6 μg μl^{-1} with Nonidet P-40 lysis buffer in spin columns (Pierce) and mixed with anti-mCherry monoclonal antibody (Clontech) and rotated at 4 °C for 2 h. Protein A/G-agarose beads (30 μl, Pierce) were added to lysate and rotated at 4 °C for 4 h. Beads were washed three times with Nonidet P-40 lysis buffer by centrifugation at 1500 × *g* for 2 min at 4 °C and protein was eluted by boiling in 2× concentrated sample buffer (1% SDS, 5% glycerol, 25 mM Tris-HCl, pH 6.8, 0.01% bromphenol blue, 0.5% 2-mercaptoethanol). Protein was resolved on a 3–8% gradient NuPAGE Tris acetate gel (Invitrogen) and transferred to nitrocellulose using iBlot (Invitrogen). Immunoblots were incubated overnight at 4 °C with either anti-mCherry monoclonal antibody (Clontech, 1:1000) or rabbit polyclonal anti-eGFP antibody (Abcam, 1:1000) in 2% fish gelatin blocking buffer. Proteins were detected using SuperSignal West

Pico Chemiluminescent Substrate kit (Pierce) or using goat anit-rabbit IRDye 800CW antibody (1:10,000) in 2% fish gelatin blocking buffer and analyzed with the Odyssey IR imaging system (LI-COR Biosciences).

Chemical Cross-linking—Chemical cross-linking was performed as described (33). Ano1-eGFP-transfected HEK293 cells were lysed in cross-linking buffer (PBS, pH 8). Protein was incubated with varying concentrations of the cross-linker 1,5-difluoro-2,4-dinotrobenzene (Pierce) (water-insoluble, membrane permeable, spacer arm length, 3 Å) at 37 °C for 10 min. The cross-linking reaction was stopped by the addition of 20 mM Tris, pH 7.5, and incubated at room temperature for 20 min. Samples were mixed with 4× NuPAGE LDS sample buffer containing 50 mM dithiothreitol (DTT) and incubated at 70 °C for 10 min. Protein was resolved on a 3–8% NuPAGE Tris acetate gels and analyzed by Western blotting.

Native PAGE—Cells were sonicated in 600 μl of native PAGE 4× sample buffer containing 2% *n*-dodecyl β-D-maltoside (Invitrogen). Lysate was centrifuged at 16,000 × *g* for 10 min at 4 °C. Supernatant was collected and 10 μg of protein was treated with varying concentrations of SDS and treated with 0.5% G-250 (Invitrogen). Protein was resolved on a Native PAGE Novex 4–16% BisTris gel and detected by Western blotting.

Electromobility Shift Assay—Whole cell HEK293 lysate expressing Ano1-eGFP and Ano1-mCherry was obtained for electromobility shift assay (EMSA) analysis. Whole cell lysate containing 7.5 μg of protein was prebound with anti-mCherry at 4 °C for 1 h. Prebound lysate was then subjected to non-denaturing PAGE. Protein shift was resolved by Western blotting with anti-GFP.

Statistical Methods—All data are presented as the mean ± S.E. for *n* number of cells. Each transfection was repeated on at least three separate days. Differences between means were tested for statistical significance using paired or unpaired *t* tests or their non-parametric equivalent as appropriate to the experiment. From such comparisons, differences yielding $p \leq 0.05$ were judged to be significant.

RESULTS

Ano Expression and Verification of Ano1 Construct Function—We have previously shown that HEK293 cells do not endogenously express a Ca^{2+}-activated Cl^- current (34). However, to determine that these cells did not endogenously express Ano1, we performed RT-PCR (Fig. 1*A*). Consistent with the lack of an endogenous CaCC (see also Fig. 1*E*), these cells did not express Ano1. However, Ano2, -4, -5, -6, -8, and -10 were endogenously expressed, suggesting that these additional Ano family members are not capable of forming a CaCC in these cells.

To probe the quaternary structure of Ano1, we fused eGFP and mCherry to the C termini of Ano1. We then verified that these FRET constructs could still be activated by intracellular Ca^{2+} to conduct Cl^-. With nominally zero intracellular Ca^{2+}, both tagged constructs and the untagged wild type Ano1 failed to display significant currents (<0.05 nA; Fig. 1*E*). However, in the presence of 1 μM free intracellular Ca^{2+}, whole cell currents were typically >5 nA for all Ano1s (Fig. 1, *B–E*). Importantly, the currents from both constructs exhibited outward rectification and time dependence that was typical of CaCC currents at this Ca^{2+} concentration and was identical to untagged Ano1 (Fig. 1, *B–E*) (35). These results

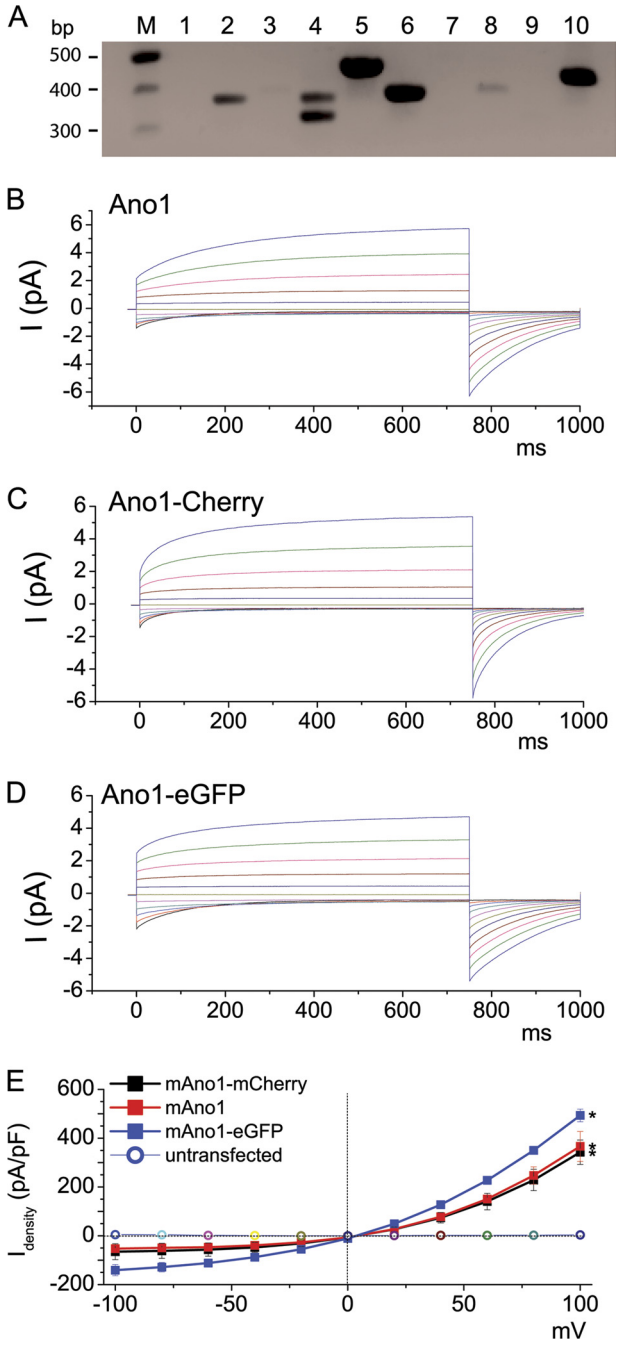

FIGURE 1. **Ca^{2+}-activated Cl^- currents induced by fluorescent protein-tagged mouse Ano1 constructs are identical to wild type Ano1.** HEK293 cells were transiently transfected and subjected 1 day later to whole cell patch clamp recording. *A*, total RNA was collected from untransfected HEK293 cells and RT-PCR was performed to determine which Ano proteins are endogenously expressed. Ano5, -6, and -10 were strongly expressed, whereas Ano2 and -4 were mildly expressed. Ano1, -3, -7, -8, and -9 were not detectable. *B*, wild type mouse Ano1 (variant containing *a* and *c* alternative splice sequences, accession Q8BHY3.2). *C*, Ano1 tagged with eGFP on the C terminus. *D*, Ano1 tagged with mCherry on the C terminus. *E*, steady-state current-voltage relationships (*red square*, wild type; *black square*, mCherry-tagged Ano1; *blue square*, eGFP-tagged Ano1; *circle*, untransfected). All $n = 10$. *N.B.*, in some cases, *error bars* were obscured by the symbols. * denotes $p < 0.05$ different to basal currents.

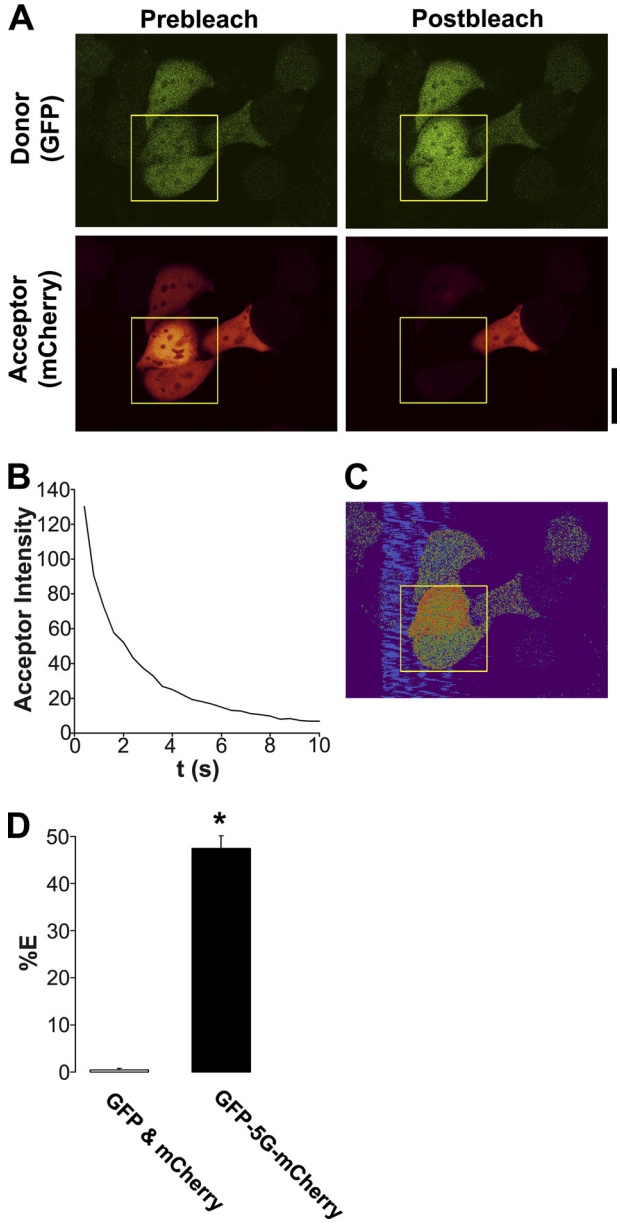

FIGURE 2. **eGFP linked to mCherry with 5 glycines (eGFP-5G-mCherry) undergoes near-maximal FRET.** *A*, typical confocal micrographs of eGFP-5G-mCherry (*green*, donor; *red*, acceptor) before and after photobleaching of the acceptor fluorophore. *B*, graph showing typical acceptor photobleaching over 10 s. *C*, resultant FRET image from *A*. *D*, mean FRET efficiency (%E) of unlinked eGFP and mCherry cotransfected in the same cells ($n = 10$) and from eGFP-5G-mCherry ($n = 14$). * denotes $p < 0.05$ different between linked and unlinked eGFP and mCherry. *Scale bar* represents 25 μm.

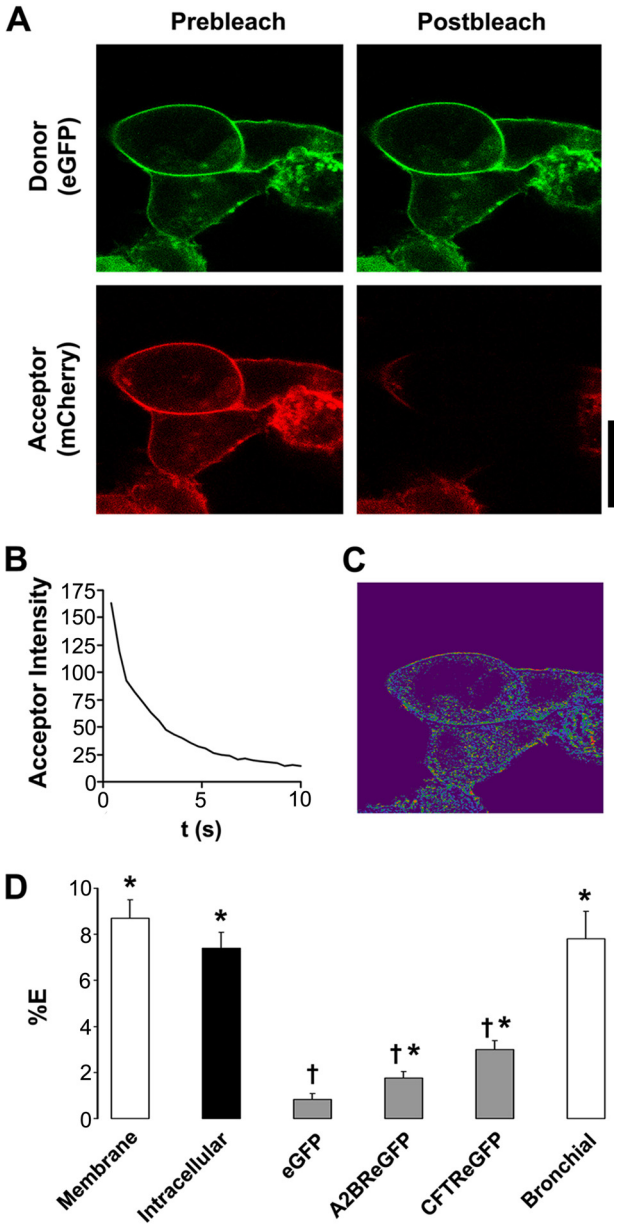

FIGURE 3. **Ano1-eGFP and Ano1-mCherry undergo specific FRET in the plasma membrane.** *A*, typical confocal micrographs of Ano1-eGFP (*green*, donor) and Ano1-mCherry (*red*, acceptor) before and after photobleaching of Ano1-mCherry. *B*, graph showing typical acceptor photobleaching over 10 s. *C*, resultant FRET image calculated from *A*. *D*, mean FRET efficiency (%E). *Open bars*, plasma membrane FRET in HEK293 cells ($n = 56$) and human bronchial epithelial cells ($n = 13$). *Closed bar*, intracellular FRET in HEK293 cells ($n = 36$). *Gray bars*, FRET between Ano1-mCherry and the denoted acceptor molecule. *eGFP*, Ano1-mCherry ($n = 19$); *A2BR-eGFP*, Ano1-mCherry ($n = 19$); *CFTR-eGFP*, Ano1-mCherry ($n = 22$). * denotes FRET that is $p < 0.05$ different from 0. † denotes FRET that is $p < 0.05$ different from plasma membrane Ano1 FRET in HEK293 cells. *Scale bar* represents 25 μm.

demonstrate that attaching eGFP or mCherry had no obvious effect on Ano1 function.

Ano1-eGFP and Ano1-mCherry Undergo FRET in the Plasma Membrane of HEK293 Cells and Airway Epithelia—We first used FRET to search for Ano1-Ano1 interactions because this method allows for live cell quantification. As a positive FRET control, we directly linked eGFP to mCherry by five glycines (in the absence of Ano1) and measured the % FRET with this construct in HEK293 cells using the acceptor photobleaching approach (36). Typical acceptor photobleaching of this FRET pair is shown in Fig. 2, *A* and *B*. We were able to measure 48 ± 1% FRET with this construct (Fig. 2, *C* and *D*), which is close to the maximal FRET that is measurable between eGFP and mCherry (50%) (37), suggesting that we can accurately measure FRET with our system. In contrast, unlinked eGFP and mCherry did not undergo FRET when co-expressed in HEK cells (Fig. 2*D*).

24 h after transfection in HEK293 cells, Ano1 was predominantly expressed in the plasma membrane (Fig. 3*A*) and after acceptor photobleaching (Fig. 3*B*) we detected a significant 8% of FRET (Fig. 3, *C* and *D*), suggesting that Ano1 subunits

were close enough to interact. To determine whether Ano1 channels associate before they reach the plasma membrane, we measured Ano1 FRET ~15 h post-transfection when more Ano1 is located intracellularly. Intracellular Ano1-eGFP − Ano1-mCherry FRET was also ~8% (Fig. 3*D*), suggesting that Ano1 oligomers assemble before reaching the plasma membrane.

We failed to detect any FRET between eGFP alone and Ano1-mCherry, suggesting that the Ano1 FRET was due to the specific assembly of Ano1 subunits. To test for the possibility that the plasma membrane of a HEK293 cell may become crowded following transient transfections, forcing an intimateness that would not normally occur, we co-expressed Ano1-mCherry and eGFP-tagged A2B adenosine receptor (A2BR-eGFP), a G-protein-coupled receptor that resides in the plasma membrane but has not previously been shown to interact with Ano1. In this case, there was a small, but significant, amount of FRET (2%), which was significantly less than the 8% FRET seen between Ano1 subunits (Fig. 3*D*). Coexpressed Ano1-mCherry and eGFP-tagged CFTR also returned moderate FRET (~3.5%) that was also significantly less than the 8% FRET seen between Ano1 subunits (Fig. 3*D*). Together, these low levels of FRET are perhaps indicative of the restricted two-dimensional diffusion that limits distances between two proteins that do not physically interact in the plasma membrane.

To demonstrate that Ano1-Ano1 FRET was not influenced by the expression system used, we co-expressed the Ano1 constructs in single primary human bronchial epithelial cells. We again observed close to 8% FRET in these cells, suggesting that the Ano1 interaction is an intrinsic property of Ano1, rather than a discreteness forced by the HEK293 expression system (Fig. 3*D*).

Ano1 FRET Is Due to a Protein-Protein Interaction—To confirm that FRET between Ano1-eGFP and Ano1-mCherry was due to a physical interaction, we co-immunoprecipitated Ano1-mCherry and Ano1-eGFP using antibodies specifically raised against eGFP and mCherry (Fig. 4*A*). As a negative control, we immunoprecipitated Ano1-mCherry from HEK293 cells co-expressing A2BR-eGFP or eGFP and probed with an eGFP antibody (Fig. 4*A*). No bands were detected after blotting for eGFP in control lanes, indicating that these proteins do not interact with Ano1. Western blotting confirmed that both antibodies are specific for eGFP/mCherry, respectively, and neither detected the other fluorescent protein (Fig. 4*B*).

Ano1 FRET Is Not Altered by Changes in Intracellular Ca^{2+} or Actin Cytoskeleton Disruption—We next tested whether changes in intracellular Ca^{2+} could alter Ano1 FRET. Intracellular Ca^{2+} was raised with 2 μM thapsigargin (17), 100 μM UTP (32), or 10 μM ionomycin (38). Cells treated with UTP were also transfected with an HA-tagged $P2Y_2$ receptor construct ($P2Y_2$R-HA) to ensure a consistent UTP response. HEK293 cells displayed a robust increase in the Fura-2 emission ratio after all three treatments (Fig. 5, *A*, *C*, and *E*). However, these maneuvers failed to affect Ano1 FRET (Fig. 5, *B*, *D*, and *F*), suggesting that Ano1-Ano1 interactions are not influenced by changes in intracellular Ca^{2+}.

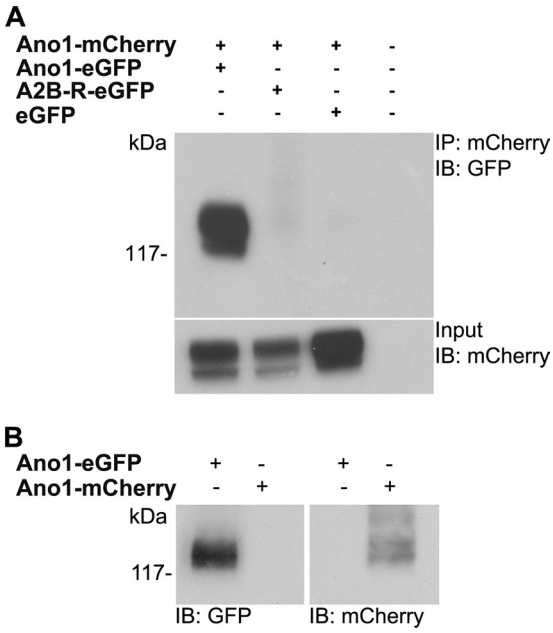

FIGURE 4. **Ano1-eGFP and Ano1-mCherry co-immunoprecipitate.** *A*, HEK293 cells were transfected with Lipofectamine alone, or with Ano1-mCherry and Ano1-eGFP, A2B-R-eGFP, and eGFP. *Input* represents 5% of total protein used in co-immunoprecipitation. *B*, Western blot indicating specificity of eGFP and mCherry antibodies. HEK293 cells were transfected with either Ano1-eGFP or Ano1-mCherry. The eGFP antibody only detected Ano1-eGFP (*left*), whereas mCherry antibody only detected Ano1-mCherry (*right*). The blot is representative of three separate experiments. *IB*, immunoblot.

Epithelial ion channels have been shown to be linked to the cytoskeletal infrastructure by postsynaptic density 95 discs largezonula occludens-1 (PDZ) binding motifs and these interactions can be ablated by disrupting F-actin polymerization with cytochalasin D (39). However, a 30-min treatment with 1 μM cytochalasin D had no effect on plasma membrane Ano1 FRET, suggesting that oligomerization of Ano1 is not contingent on binding to the actin cytoskeleton (Fig. 6).

Biochemical Evidence That Ano1 Is a Dimer—To investigate the stoichiometry of Ano1, we performed chemical cross-linking experiments on cell lysates obtained from HEK293 cells expressing Ano1-eGFP (Fig. 7*A*). Under control (*i.e.* reducing) conditions, Ano1-eGFP was seen predominantly as a ~130 kDa monomer. However, after treating whole cell lysate with the cross-linker 1,5-difluoro-2,4-dinotrobenzene, an additional band was observed that corresponded to an Ano1-eGFP dimer (~260 kDa). Two faint higher order bands were also visible. However, the molecular weight of these bands was harder to ascertain and may represent nonspecific cross-linking of Ano1 to other membrane proteins.

We next performed non-denaturing PAGE on lysate obtained from HEK293 cells to validate the cross-linking experiments (Fig. 7*B*). Cells were lysed by 2% *n*-dodecyl β-D-maltoside and sonicated in the absence of SDS. The majority of Ano1 appeared as a dimer with no presence of higher order bands. Inclusion of SDS induced the emergence of a ~117 kDa band indicating that Ano1 had been fully denatured and that we were observing the monomeric protein. This band was slightly smaller than the predicted size of Ano1-eGFP

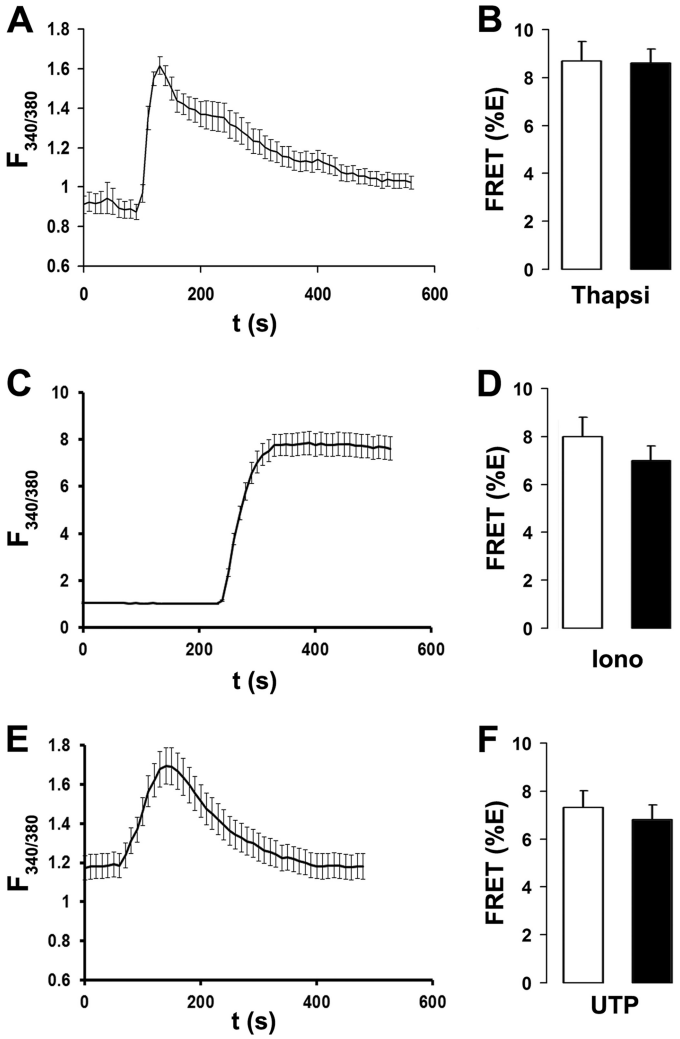

FIGURE 5. **Ano1-eGFP and Ano1-mCherry FRET are not affected by changes in intracellular Ca^{2+}.** *A*, typical Fura-2 emission ratio observed following exposure to 2 μM thapsigargin ($n = 10$). *B*, mean FRET (%E) from Ano1 in the plasma membrane of HEK293 cells after vehicle (*open bars*, $n = 25$) and following a 5-min exposure to 2 μM thapsigargin (*closed bars*, $n = 27$). *C*, typical Fura-2 emission ratio observed following exposure to 1 μM ionomycin ($n = 10$). *D*, mean FRET (%E) from Ano1 in the plasma membrane of HEK293 cells after vehicle (*open bars*, $n = 20$) and following a 5-min exposure to 1 μM ionomycin (*closed bars*, $n = 21$). *E*, typical Fura-2 emission ratio observed following exposure to 10 μM UTP ($n = 10$). *F*, mean FRET (%E) from Ano1 in the plasma membrane of HEK293 cells after vehicle (*open bars*, $n = 20$) and following a 5-min exposure to 10 μM UTP (*closed bars*, $n = 20$).

(~130 kDa), but is consistent with an apparent reduction in protein size seen under non-reducing conditions (40). To ensure that we were observing Ano1-eGFP dimers and not Ano1-eGFP in association with an unidentified endogenous protein, we performed an EMSA by exposing lysate from HEK293 cells expressing Ano1-eGFP and Ano1-mCherry to an mCherry antibody before non-denaturing PAGE (Fig. 7*C*). We then blotted for eGFP to test whether Ano1-eGFP was shifted to a higher molecular weight by antibody pre-binding. A portion of Ano1-eGFP remained at 230 kDa, which likely represented a homodimer population of Ano1-eGFP alone. Importantly, we observed a distinct shift of Ano1-eGFP to a higher molecular weight, which corresponded to a complex containing Ano1-eGFP, Ano1-mCherry, and the mCherry antibody.

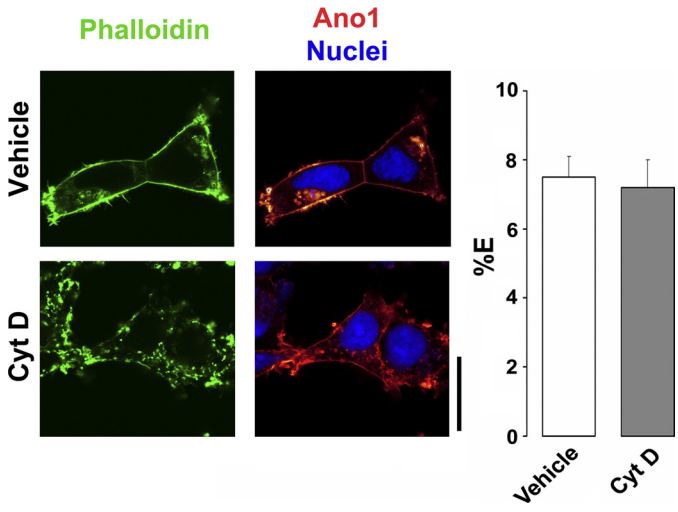

FIGURE 6. **Ano1-eGFP and Ano1-mCherry FRET are not dependent on an intact actin cytoskeleton.** *Left*, confocal micrographs of Ano1-mCherry in HEK293 cells (*red*) before and after disruption of actin cytoskeleton (phalloidin/green) with 1 μM cytochalasin D for 30 min. *Right*, mean % E in HEK293 cells after vehicle (*open bars*, $n = 36$) and after 30 min cytochalasin D (*Cyt D*) exposure (*gray bars*, $n = 49$). *Scale bar* represents 25 μm.

DISCUSSION

We examined the stoichiometry of Ano1 using biophysical and biochemical approaches. We used HEK293 cells because they do not endogenously express Ano1 (Fig. 1*A*) and do not have a spontaneously active CaCC, even with 1 μM Ca^{2+} in the patch pipette (Fig. 1*E*). For our studies, we C-terminally labeled murine Ano1 with either eGFP or mCherry. To ensure that these fluorescent proteins did not interfere with Ano1 function, we included a 17-amino acid linker between Ano1 and eGFP or mCherry. Importantly, these fluorescent proteins had no effect on Ano1-mediated Cl^- currents, suggesting that their use in this endeavor was valid (Fig. 1).

We chose eGFP/mCherry over the more commonly used CFP/YFP FRET pair because CFP photobleaches easily, which reduces its ability to donate photons during FRET, whereas eGFP is significantly more photostable (41). This approach was confirmed using a FRET-positive construct where the acceptor was linked to the donor by 5 glycines (Fig. 2). The theoretical maximum FRET that can occur between two fluorescent proteins (including CFP, eGFP, mCherry, and YFP) is 50%, which is limited by the size of the fluorescent proteins themselves (37). Using CFP linked to YFP, we measured 38 ± 3% FRET ($n = 6$). In contrast, we measured 48 ± 1% FRET ($n = 14$) with eGFP linked to mCherry, confirming previous reports that the latter FRET pair is significantly more suited for confocal microscopy (Fig. 2) (41).

Using acceptor-photobleaching FRET, we found a remarkably constant 8% FRET between Ano1-eGFP − Ano1-mCherry (Fig. 3), which suggested that Ano1 can oligomerize. Co-immunoprecipitation experiments revealed that Ano1-eGFP and Ano1-mCherry are associated. In contrast, Ano1-mCherry did not co-immunoprecipitate with A2BR-eGFP, suggesting that the observed 2% FRET between these proteins was due to the moderate proximity in the plasma membrane, and not a direct physical interaction. Many other apical membrane ion channels are known to oligomerize. For example,

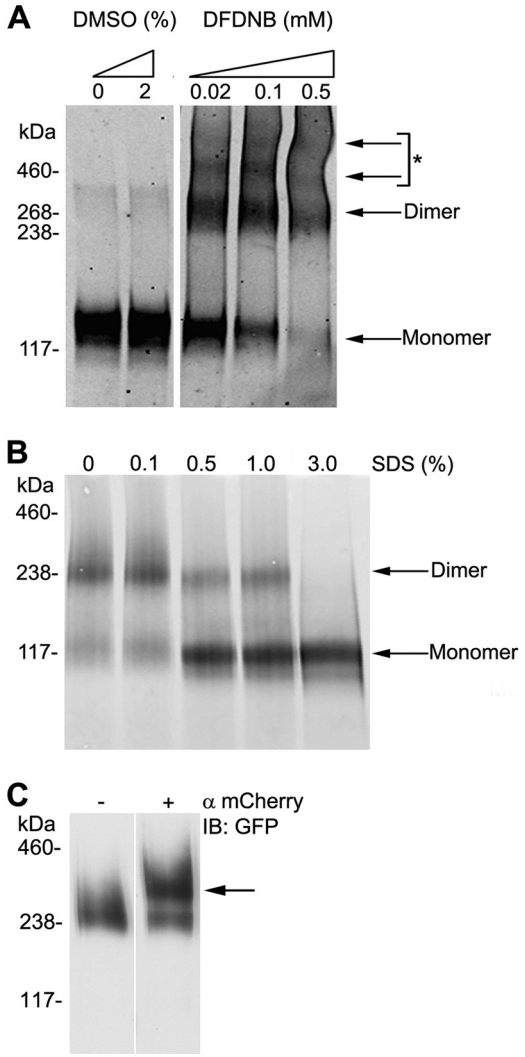

FIGURE 7. **Determination of Ano1 subunit stoichiometry by chemical cross-linking and non-denaturing gel electrophoresis.** *A*, determination of possible oligomeric structures of Ano1-eGFP using chemical cross-linking. Cell lysates were treated with increasing concentrations of 1,5-difluoro-2,4-dinotrobenzene, membrane permeable (*DFDNB*). *, denotes possible higher order complexes or adducts. *B*, determination of oligomeric structure of Ano1-eGFP under non-denaturing (native) PAGE conditions. Cell lysates were incubated with 0–3% of SDS to denature protein complexes and probed. Under non-denaturing conditions, Ano1 is found mainly as a dimer. *C*, EMSA analysis from HEK293 cell lysate expressing Ano1-eGFP and Ano1-mCherry, showing a mobility shift elicited by anti-mCherry (*arrow*). *IB*, immunoblot.

ENaC is a heteromultimer that returns between 5 and 15% FRET between different ENaC subunits (42). ENaC is also known to interact with CFTR (43) and FRET was 7% between CFTR and all three ENaC subunits (43). A study by Kerschensteiner *et al.* (44) used acceptor-photobleaching FRET to determine the stoichiometry of voltage-gated K^+ (Kv) channels that are known to be heteromeric oligomers. They obtained ~25% FRET efficiency when Kv2.1-CFP and Kv9.3-YFP were expressed compared with a ~10% FRET efficiency when Kv2.1-YFP and Kv9.3-CFP were expressed. Thus, the 8% FRET that we record between Ano1 subunits is comparable with both FRET seen between ion channel subunits and between distinct ion channels. Perhaps, surprisingly, whereas CFTR has previously been shown to negatively regulate CaCC (45, 46), we detected only minimal FRET between CFTR and Ano1 (Fig. 3), suggesting that regulation of Ano1 by CFTR is not due to a direct interaction. Because we found Ano1-Ano1 FRET to be 8% when measured intracellularly (Fig. 3), it is likely that Ano1 subunits come together *en route* to the plasma membrane. It should be noted that we did not differentiate between intracellular compartments during our analysis and subunits may oligomerize as early as the ER or as late as endosomes.

CFTR indirectly binds to the actin cytoskeleton via its C-terminal PDZ-binding motif and disruption of F-actin polymerization with cytochalasin D affects CFTR activity (47, 48). Performing a computational search with the Eukaryotic Linear Motif resource, we found that murine Ano1 also has a predicted C-terminal PDZ-binding motif (GDAL), which may serve to link Ano1 to the actin cytoskeleton through intermediary scaffolding proteins. However, the ability of Ano1 to undergo FRET was not affected by cytochalasin D exposure, suggesting that Ano1 subunit interactions are not cytoskeleton-dependent (Fig. 6). However, the effect of cytochalasin D on trafficking remains to be determined. We also found Ano1 FRET to be insensitive to intracellular Ca^{2+} levels (Fig. 5), suggesting that Ano1 oligomerization is fixed and independent of the gating ability of Ano1, which is Ca^{2+}-dependent (11–13).

Chemical cross-linking and non-denaturing PAGE assays indicated that Ano1 is a dimer (Fig. 7). A distinct dimer band was observed following chemical cross-linking (Fig. 7*A*), which was not observed under control conditions. Additional higher order complexes were also observed after cross-linking. However, these may be proteins that are non-specifically cross-linked to Ano1-eGFP. Following non-denaturing PAGE a strong dimer band was also observed (Fig. 7*B*). This dimerization was only disrupted with 3% SDS (Fig. 7*B*). Higher order oligomers were not detected by non-denaturing PAGE, suggesting those observed following cross-linking are not true oligomers. We next performed EMSA to determine whether the dimer band consists of two Ano1 proteins or Ano1 with an unidentified endogenous protein (Fig. 7*C*). This approach revealed a shift of Ano1-eGFP to a higher molecular weight when prebound with an anti-mCherry antibody, confirming that Ano1-eGFP was present as a dimer with Ano1-mCherry and not with any other protein. Because only Ano1 is present under non-denaturing conditions, it is likely that the co-immunoprecipitation is indicative of a direct interaction between Ano1 subunits (Fig. 4). A portion of Ano1-eGFP did not shift to a higher molecular weight. This is likely due to the fact that HEK293 cells transfected with Ano1-eGFP and Ano1-mCherry should yield three distinct populations of Ano1 dimers, consisting of Ano1-eGFP/Ano1-eGFP, Ano1-eGFP/Ano1-mCherry, and Ano1-mCherry/Ano1-mCherry.

Although Ano1 has been identified as an essential subunit of CaCC (11–13), transiently expressed Ano1 could form a heteromultimer with other anoctamin family members because many of these proteins are ubiquitously expressed (Fig. 1*A*). However, our data suggests that this is not the case and that Ano1 specifically forms a homodimer and in conclusion, we have shown that Ano1-eGFP and Ano1-mCherry are func-

tional proteins that form a dimer. Determining the oligomeric structure of CaCC is an important step toward a better understanding of how this recently identified channel functions. Further work is needed to determine how Ano1 subunits come together, whether other proteins facilitate the process, and how this affects activation of CaCC and conductance of Cl^-.

Acknowledgments—The mouse Ano1 clone used in these studies was kindly provided by Dr. Uhtaek Oh (Seoul National University, Korea). The technical support of Michael Watson and Nancy Quiney is gratefully acknowledged.

REFERENCES

1. Eggermont, J. (2004) *Proc. Am. Thorac. Soc.* **1,** 22–27
2. Hengl, T., Kaneko, H., Dauner, K., Vocke, K., Frings, S., and Möhrlen, F. (2010) *Proc. Natl. Acad. Sci. U.S.A.* **107,** 6052–6057
3. Rasche, S., Toetter, B., Adler, J., Tschapek, A., Doerner, J. F., Kurtenbach, S., Hatt, H., Meyer, H., Warscheid, B., and Neuhaus, E. M. (2010) *Chem. Senses* **35,** 239–245
4. Stephan, A. B., Shum, E. Y., Hirsh, S., Cygnar, K. D., Reisert, J., and Zhao, H. (2009) *Proc. Natl. Acad. Sci. U.S.A.* **106,** 11776–11781
5. Stöhr, H., Heisig, J. B., Benz, P. M., Schöberl, S., Milenkovic, V. M., Strauss, O., Aartsen, W. M., Wijnholds, J., Weber, B. H., and Schulz, H. L. (2009) *J. Neurosci.* **29,** 6809–6818
6. Large, W. A., and Wang, Q. (1996) *Am. J. Physiol. Cell Physiol.* **271,** C435–454
7. Duan, D. (2009) *J. Physiol.* **587,** 2163–2177
8. Liu, B., Linley, J. E., Du, X., Zhang, X., Ooi, L., Zhang, H., and Gamper, N. (2010) *J. Clin. Invest.* **120,** 1240–1252
9. Barish, M. E. (1983) *J. Physiol.* **342,** 309–325
10. Miledi, R. (1982) *Proc. R. Soc. Lond. B. Biol. Sci.* **215,** 491–497
11. Caputo, A., Caci, E., Ferrera, L., Pedemonte, N., Barsanti, C., Sondo, E., Pfeffer, U., Ravazzolo, R., Zegarra-Moran, O., and Galietta, L. J. (2008) *Science* **322,** 590–594
12. Schroeder, B. C., Cheng, T., Jan, Y. N., and Jan, L. Y. (2008) *Cell* **134,** 1019–1029
13. Yang, Y. D., Cho, H., Koo, J. Y., Tak, M. H., Cho, Y., Shim, W. S., Park, S. P., Lee, J., Lee, B., Kim, B. M., Raouf, R., Shin, Y. K., and Oh, U. (2008) *Nature* **455,** 1210–1215
14. Huang, F., Rock, J. R., Harfe, B. D., Cheng, T., Huang, X., Jan, Y. N., and Jan, L. Y. (2009) *Proc. Natl. Acad. Sci. U.S.A.* **106,** 21413–21418
15. Rock, J. R., O'Neal, W. K., Gabriel, S. E., Randell, S. H., Harfe, B. D., Boucher, R. C., and Grubb, B. R. (2009) *J. Biol. Chem.* **284,** 14875–14880
16. Romanenko, V. G., Catalán, M. A., Brown, D. A., Putzier, I., Hartzell, H. C., Marmorstein, A. D., Gonzalez-Begne, M., Rock, J. R., Harfe, B. D., and Melvin, J. E. (2010) *J. Biol. Chem.* **285,** 12990–13001
17. Lytton, J., Westlin, M., and Hanley, M. R. (1991) *J. Biol. Chem.* **266,** 17067–17071
18. Zhu, M. H., Kim, T. W., Ro, S., Yan, W., Ward, S. M., Koh, S. D., and Sanders, K. M. (2009) *J. Physiol.* **587,** 4905–4918
19. Schreiber, R., Uliyakina, I., Kongsuphol, P., Warth, R., Mirza, M., Martins, J. R., and Kunzelmann, K. (2010) *J. Biol. Chem.* **285,** 7838–7845
20. Pifferi, S., Dibattista, M., and Menini, A. (2009) *Pflugers Arch.* **458,** 1023–1038
21. Das, S., Hahn, Y., Walker, D. A., Nagata, S., Willingham, M. C., Peehl, D. M., Bera, T. K., Lee, B., and Pastan, I. (2008) *Cancer Res.* **68,** 6306–6312
22. Duran, C., Thompson, C. H., Xiao, Q., and Hartzell, H. C. (2010) *Annu. Rev. Physiol.* **72,** 95–121
23. Schwappach, B. (2008) *Mol. Membr. Biol.* **25,** 270–278
24. Kuo, M. M., Baker, K. A., Wong, L., and Choe, S. (2007) *Proc. Natl. Acad. Sci. U.S.A.* **104,** 2151–2156
25. Cui, J., Yang, H., and Lee, U. S. (2009) *Cell Mol. Life Sci.* **66,** 852–875
26. Hwang, T. C., and Sheppard, D. N. (2009) *J. Physiol.* **587,** 2151–2161
27. Chen, J. H., Chang, X. B., Aleksandrov, A. A., and Riordan, J. R. (2002) *J. Membr. Biol.* **188,** 55–71
28. Ramjeesingh, M., Kidd, J. F., Huan, L. J., Wang, Y., and Bear, C. E. (2003) *Biochem. J.* **374,** 793–797
29. Weatherman, R. V., Chang, C. Y., Clegg, N. J., Carroll, D. C., Day, R. N., Baxter, J. D., McDonnell, D. P., Scanlan, T. S., and Schaufele, F. (2002) *Mol. Endocrinol.* **16,** 487–496
30. Sromek, S. M., and Harden, T. K. (1998) *Mol. Pharmacol.* **54,** 485–494
31. Xiao, Q., Yu, K., Cui, Y. Y., and Hartzell, H. C. (2009) *J. Physiol.* **587,** 4379–4391
32. Tarran, R., Loewen, M. E., Paradiso, A. M., Olsen, J. C., Gray, M. A., Argent, B. E., Boucher, R. C., and Gabriel, S. E. (2002) *J. Gen. Physiol.* **120,** 407–418
33. Penna, A., Demuro, A., Yeromin, A. V., Zhang, S. L., Safrina, O., Parker, I., and Cahalan, M. D. (2008) *Nature* **456,** 116–120
34. Fischmeister, R., and Hartzell, H. C. (2005) *J. Physiol.* **562,** 477–491
35. Kuruma, A., and Hartzell, H. C. (2000) *J. Gen. Physiol.* **115,** 59–80
36. Kenworthy, A. K. (2001) *Methods* **24,** 289–296
37. Albertazzi, L., Arosio, D., Marchetti, L., Ricci, F., and Beltram, F. (2009) *Photochem. Photobiol.* **85,** 287–297
38. Ribeiro, C. M., McKay, R. R., Hosoki, E., Bird, G. S., and Putney, J. W., Jr. (2000) *Cell Calcium* **27,** 175–185
39. Lamprecht, G., and Seidler, U. (2006) *Am. J. Physiol. Gastrointest. Liver Physiol.* **291,** G766–777
40. Wittig, I., and Schägger, H. (2008) *Proteomics* **8,** 3974–3990
41. Tramier, M., Zahid, M., Mevel, J. C., Masse, M. J., and Coppey-Moisan, M. (2006) *Microsc. Res. Tech.* **69,** 933–939
42. Staruschenko, A., Medina, J. L., Patel, P., Shapiro, M. S., Booth, R. E., and Stockand, J. D. (2004) *J. Biol. Chem.* **279,** 27729–27734
43. Berdiev, B. K., Cormet-Boyaka, E., Tousson, A., Qadri, Y. J., Oosterveld-Hut, H. M., Hong, J. S., Gonzales, P. A., Fuller, C. M., Sorscher, E. J., Lukacs, G. L., and Benos, D. J. (2007) *J. Biol. Chem.* **282,** 36481–36488
44. Kerschensteiner, D., Soto, F., and Stocker, M. (2005) *Proc. Natl. Acad. Sci. U.S.A.* **102,** 6160–6165
45. Johnson, L. G., Boyles, S. E., Wilson, J., and Boucher, R. C. (1995) *J. Clin. Invest.* **95,** 1377–1382
46. Wei, L., Vankeerberghen, A., Cuppens, H., Cassiman, J. J., Droogmans, G., and Nilius, B. (2001) *Pflugers Arch.* **442,** 280–285
47. Fischer, H., Illek, B., and Machen, T. E. (1995) *J. Physiol.* **489,** 745–754
48. Haggie, P. M., Stanton, B. A., and Verkman, A. S. (2004) *J. Biol. Chem.* **279,** 5494–5500